Journal of Power Sources 196 (2011) 10526–10531

Contents lists available at ScienceDirect

Journal of Power Sources

journal homepage: www.elsevier.com/locate/jpowsour

The effect of a blocking layer on the photovoltaic performance in CdS quantum-dot-sensitized solar cells

Jongmin Kim, Hongsik Choi, Changwoo Nahm, Joonhee Moon, Chohui Kim, Seunghoon Nam, Dae-Ryong Jung, Byungwoo Park*

WCU Hybrid Materials Program, Department of Materials Science and Engineering, Research Institute of Advanced Materials, Seoul National University, Seoul 151-744, Republic of Korea

ARTICLE INFO

Article history:
Received 12 June 2011
Received in revised form 9 August 2011
Accepted 10 August 2011
Available online 17 August 2011

Keywords:
Quantum-dot-sensitized solar cells
Cadmium sulfide
Blocking layer
Charge-transfer kinetics
Trap states

ABSTRACT

In order to reduce the surface recombination at the interface between the fluorine-doped tin oxide (FTO) substrate and the polysulfide electrolyte in CdS quantum-dot-sensitized solar cells (QDSCs), compact TiO_2 is deposited on the FTO electrode by sputtering. The TiO_2-coated CdS-sensitized solar cell exhibits enhanced power-conversion efficiency (0.52%) compared with a bare CdS-sensitized solar cell (0.23%). Charge-transfer kinetics are analyzed by impedance spectroscopy, open-circuit decay, and cyclic voltammetry. The TiO_2 layer deposited on the FTO substrate acts as a blocking layer, which plays a significant role in reducing the electron back transfer from the FTO to the polysulfide electrolyte. Interestingly, with respect to the incident photon-to-current conversion efficiency (IPCE) data, asymmetric enhancement is observed from the sample with a thicker blocking layer. This is because CdS quantum dots absorb ultraviolet light completely with the TiO_2 layer because of the high extinction coefficient of the CdS quantum dots compared with dye molecules.

1. Introduction

Dye-sensitized solar cells (DSSCs) have been considered as one of the most renewable solar energy sources due to their low cost, high durability, and potential use as flexible devices. Since Grätzel and O'Regan invented the dye-sensitized nanocrystalline TiO_2 solar cell structure [1], enormous progress has been made in the power conversion efficiency of DSSCs, and maximum efficiencies of up to 11% have been achieved [2].

Recently, semiconductor quantum dots have been considered as a fascinating alternative to organic dye molecules. Quantum-dot-sensitized solar cells (QDSCs) have potential advantages over DSSCs, such as higher absorption coefficients compared with dye molecules, tailored absorptions by changing the size of quantum dots, and the possibility of exceeding the Schottky–Queisser limit by using multiple-electron generation [3–7].

Nevertheless, the QDSCs still have exhibited lower efficiencies compared with DSSCs [8]. One of the main reasons is the recombination loss due to various defects at the interfaces [9,10]. Therefore, to obtain the improved photovoltaic performance of QDSCs, studies on interface quality are necessary [11,12]. Several groups have examined the surface-treatment effects on QDSC performance [13–16], even though the exact enhancement mechanisms have not been clarified yet.

In DSSCs, the compact blocking layer was used to prevent the backward electron transfer from FTO to the conventional iodide electrolyte, and many groups have studied several materials for this layer, including TiO_2 and Nb_2O_5 [17–19]. The blocking-layer incorporation, however, induces little effect on the photovoltaic performance, because the shunt resistance of DSSCs is on the order of $10^3\ \Omega\,cm^2$ when using an iodide electrolyte [20], and this magnitude of resistance is high enough to operate DSSCs.

In the case of QDSCs, to solve the corrosion problem of quantum dots in the electrolyte [21], a polysulfide solution was used as an alternative for the $3I^-/I_3^-$ electrolyte. The fill factor of QDSCs using the polysulfide electrolyte is lower than those of DSSCs due to both the low shunt resistance of the interfaces and the high series resistance of the electrolyte [22]. One of the possible reason for the low shunt resistance is the loss caused by the recombination at the FTO/polysulfide electrolyte interfaces. Nevertheless, the mechanisms and charge-transfer kinetics of the FTO/polysulfide electrolyte have not yet been studied. In this article, we examined the influence of a TiO_2 blocking layer on the photovoltaic performance of QDSCs. The electron recombination and charge-transfer kinetics were analyzed for the recombination reactions at the FTO/polysulfide electrolyte interfaces.

* Corresponding author. Tel.: +82 2 880 8319; fax: +82 2 885 9671.
E-mail address: byungwoo@snu.ac.kr (B. Park).

0378-7753/$ – see front matter © 2011 Elsevier B.V. All rights reserved.
doi:10.1016/j.jpowsour.2011.08.052

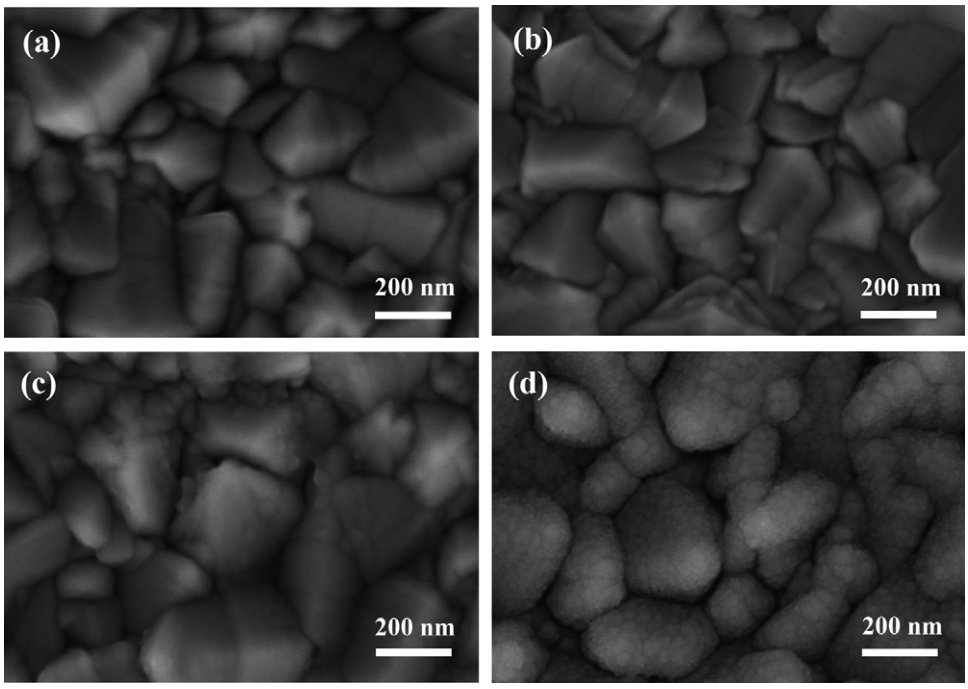

Fig. 1. Plan-view FE-SEM images of the bare and TiO_2 blocking-layer coated FTO electrode: (a) FTO substrate, (b) FTO/TiO_2 (7 nm), (c) FTO/TiO_2 (30 nm), and (d) FTO/TiO_2 (170 nm).

2. Experimental procedure

The TiO_2 blocking layer on the FTO electrode was prepared using a rf-magnetron sputtering system. The deposition was performed at room temperature (RT) under an Ar atmosphere with an operating pressure of 3 mTorr and rf power of 100 W. The thickness of the blocking layer was controlled by changing the deposition time in the range of 5–120 min. Commercial TiO_2 nanopowder (Ti-Nanoxide D; Solaronix, Switzerland) was used as a host material for QDSCs. The paste was spread with a one-step doctor blade method on the fluorine-doped tin oxide (FTO, TEC 8; Pilkington, Japan) electrode, and the paste-coated electrodes were subsequently annealed at 450 °C for 30 min in ambient air. The thickness of the TiO_2 nanoparticle layer was approximately 5 μm, and the active area of the photoelectrode was 0.28 cm^2.

The CdS quantum dots were coated onto the TiO_2 nanoparticle electrode using a successive ionic-layer adsorption and reaction (SILAR) method for fabricating efficient QDSCs with high quantum-dot coverage [23,24]. The as-prepared TiO_2 electrodes were immersed in 0.04 M cadmium chloride ($CdCl_2$; Aldrich, St. Louis, USA) in methanol for 1 min, and then the same samples were soaked in 0.04 M sodium sulfide (Na_2S; Aldrich, St. Louis, USA) dissolved in methanol. Following each step, the electrodes were rinsed with methanol for 1 min and dried. This coating process was repeated five times. The polysulfide electrolyte was prepared by dissolving 0.5 M Na_2S, 1 M S, and 0.02 M KCl in methanol/water with the ratio of 7:3 solutions [24]. The Pt counter electrode was deposited on the FTO substrate by rf-magnetron sputtering. Thermoplastic foil (25 μm; Dupont, France) was used as a spacer for the sandwich-type solar cells.

The photocurrent–voltage (*J–V*) curves were characterized with a solar cell measurement system (K3000: McScience, Korea) under a solar simulator (Xenon lamp, air mass (AM) 1.5, 100 mW cm^{-2}). Impedance spectra and open-circuit decay measurements were performed using a potentiostat (CHI 608C: CH Instrumental Inc., Austin, USA) and solar simulator (PEC-L11: Peccell, Japan) under AM 1.5 illumination. The electrochemical impedance spectra were recorded over a frequency range of 0.1 to 10^5 Hz. An electrochemical analyzer (CHI 604A: CH Instrumental Inc., Austin, USA) was used for measuring the electrochemical reactions at the FTO/electrolyte interface. Field-emission scanning electron microscopy (FE-SEM, SU70: Hitachi, Japan) was used to characterize the morphology of the blocking layer on the FTO electrode. The absorption spectra of the blocking-layer coated FTO were recorded on a UV/Vis spectrophotometer (Lambda 20: Perkin-Elmer, Waltham, USA) with bare FTO as a reference. Incident photon-to-current conversion efficiency (IPCE) was obtained by using an IPCE measurement system (K3100: McScience, Korea).

3. Results and discussion

Fig. 1 shows the plan-view FE-SEM images of the bare and TiO_2 blocking layer coated on the FTO electrode. The film morphology and coverage changed with the deposition time. The nominal thicknesses of all the blocking layers are 7, 30, and 170 nm, depending on the deposition rate of the TiO_2 film. The island growth is clearly observed from the 30 nm-TiO_2 blocking layer on FTO, and after the 170 nm deposition, the FTO substrate is completely covered with the TiO_2 layer.

From the current density–voltage (*J–V*) curves of the CdS-sensitized solar cells in Fig. 2, the photovoltaic-conversion efficiencies of the cells are enhanced with increases in the TiO_2 blocking-layer thickness, and both the open-circuit voltage and short-circuit current also increased. The fill factor showed maximum with the 7 nm-deposited cell, and gradually decreased with the increasing blocking-layer thickness. The possible reasons are the resistance of the blocking layer itself that impedes electron transport from TiO_2 nanoparticles to the FTO substrate [9,17], or inefficient ion transport of the polysulfide electrolyte as the flux of current increases [25].

As shown in Table 1, the 30 nm-deposited cell exhibits the best efficiency, by more than a factor of two compared to the bare cell. On the other hand, the thick blocking layer results in a decreased conversion efficiency.

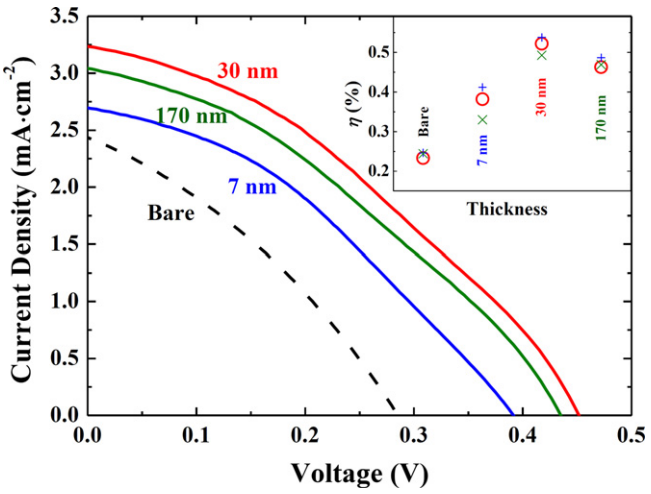

Fig. 2. Photocurrent density–voltage characteristics of CdS-sensitized solar cells with various blocking-layer thicknesses. The inset shows the power-conversion efficiency of QDSCs as a function of the blocking-layer thickness.

The open-circuit voltage (V_{oc}) and short-circuit current (J_{sc}) were affected by the TiO_2 conduction-band position, electron concentration in the TiO_2-nanoparticle layer, light-harvesting efficiency, etc. [26–28]. The conduction band of the mesoscopic TiO_2 film does not change because the TiO_2 nanoparticle/polysulfide electrolyte interface is not affected by the addition of the blocking layer. This demonstrates conclusively that the increase of V_{oc} is attributed to the increase in electron concentration which is influenced by the reduced recombination properties during light harvesting. Thus, the first aim of our study focused on the recombination properties with respect to variation of the blocking-layer thickness.

We performed dark current experiments, as shown in Fig. S1. As expected, the dark-recombination current decreases as the blocking-layer thickness increases in the positive-bias area, and the exchange current also decreased in the negative-bias region. Furthermore, compared with the poor junction characteristics of the bare sample, the coated sample exhibits good junction quality with a small leakage current [29]. The TiO_2 layer acts as the blocking layer which attenuates the charge-transfer rate at the FTO/polysulfide interface. The reduced recombination rate leads to an upward shift of the electron quasi-Fermi level E_{Fn} by increasing the electron-carrier concentration, thereby resulting in the improvement of the open-circuit voltage [30].

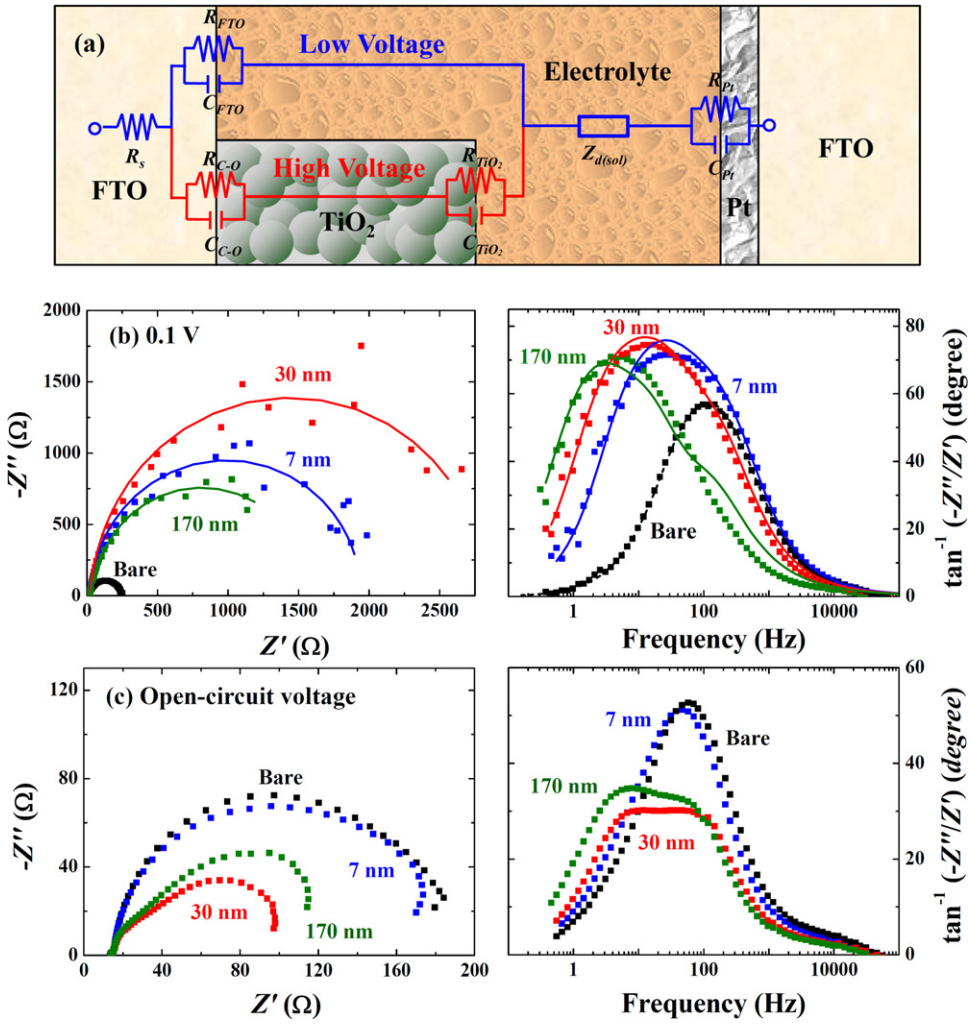

Fig. 3. (a) Equivalent circuit of QDSCs approximated for the low-voltage or high-voltage region [34]. (b) Electrochemical impedance spectroscopy for the bare and blocking-layer coated QDSCs with an applied voltage of 0.1 V, and the corresponding Bode plot. The lines were calculated using the equivalent circuit above. (c) Electrochemical impedance spectroscopy at the open-circuit voltage and the corresponding Bode plot.

Table 1
Open-circuit voltage, short-circuit current, fill factor, and power-conversion efficiency of the CdS-QDSCs with various blocking-layer thicknesses.

	V_{oc} (V)	J_{sc} (mA cm^{-2})	FF	η
Bare	0.285	2.43	33.6%	0.23%
7 nm	0.390	2.70	36.2%	0.38%
30 nm	0.451	3.24	35.7%	0.52%
170 nm	0.435	3.04	35.0%	0.46%

Electrical impedance spectroscopy (EIS) is a powerful tool for analyzing the electrochemical reaction at the interfaces [31–33]. At relatively low voltages, the Fermi level of nanoparticle TiO_2 electrode is far below the conduction band. So, the electron concentration in the TiO_2 electrode is relatively low, and the nanoparticle layer behaves like an insulator. Therefore, charge transfer is dominated by the reaction at the FTO/electrolyte interface [34]. Thus, we can mainly focus on the blocking-layer effect at this low-voltage region. Fig. 3(b) shows the impedance spectroscopy for the bare and blocking-layer coated QDSCs at 0.1 V with AM 1.5 illumination. The charge-transfer resistance was calculated using the equivalent-circuit model represented by Fabregat-Santiago et al. [35], as shown in Fig. 3(a). The R_s is a series resistance of FTO, R_{FTO} is the charge-transfer resistance for the electron recombination from the FTO to the electrolyte, and C_{FTO} is the capacitance for the FTO/electrolyte interface. The $Z_{d(sol)}$ stands for the impedance of diffusion in the polysulfide electrolyte, R_{Pt} is the charge-transfer resistance from the electrolyte to the Pt counter electrode, and C_{Pt} is the corresponding interfacial capacitance. The fitting lines are shown as solid/dashed lines in Fig. 3(b), and the fitting parameters are listed in Table 2. The parameters, including $Z_{d(sol)}$, R_{Pt}, and C_{Pt}, remain unchanged with the addition of the blocking layer, so these parameters are fixed. As shown in Table 2, the charge-transfer resistance increases considerably by one order of magnitude with the incorporation of the TiO_2 blocking layer, which means that the recombination is reduced at the FTO/electrolyte interface. The 170 nm-deposited sample exhibits a C_{FTO} value that is approximately five times larger than the other samples, due to the capacitive charging/discharging of the thick TiO_2 blocking layer on the FTO. As shown in the Bode plot, the peak frequency is shifted from ~100 Hz to ~10 Hz with the addition of the blocking layer, which again indicates a reduced charge-transfer rate [36]. In spite of the low charge-transfer resistance of the 170 nm sample compared with that of the 30 nm sample, the peak-frequency position of the sample is shifted to a much lower region, and this result is in good agreement with the larger C_{FTO} value.

For the open-circuit voltage, the charge-transfer resistance of the blocking-layer coated sample exhibits lower resistance compared with the value measured at 0.1 V (Fig. 3(c)), because the electron-carrier density in the TiO_2 nanoparticles is high at the relatively high open-circuit voltage. On the other hand, the bare sample exhibits a similar resistance and Bode-plot characteristics at 0.1 V and at the open-circuit voltage, due to the relatively low open-circuit voltage of the bare sample (0.285 V), so the charge-transfer kinetics do not change significantly [35].

Table 2
Charge-transfer resistance and capacitance for the FTO/electrolyte interface of the CdS-QDSCs obtained by using an equivalent circuit at an applied voltage of 0.1 V with various blocking-layer thicknesses, based on fitting the impedance spectroscopy in Fig. 3(b).

	R_{FTO} (Ω)	C_{FTO} (μF)
Bare	181	32.6
7 nm	1881	29.4
30 nm	2768	50.0
170 nm	1511	198.7

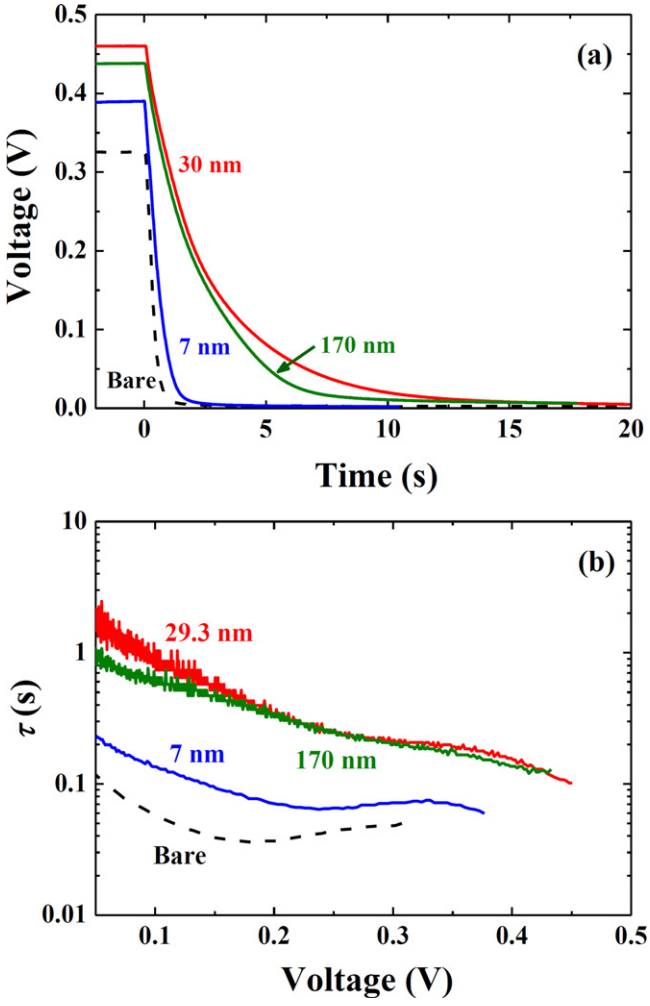

Fig. 4. (a) Experimental decay results of V_{oc} of the CdS-sensitized solar cells with various blocking-layer thicknesses. (b) The electron lifetime from Eq. (1) as a function of voltage.

The recombination rates of QDSCs were determined by photovoltaic-decay measurements. The photovoltaic-decay rate of the cell with a blocking layer exhibits much slower rate than that of the bare sample, as shown in Fig. 4(a). The electron recombination rate at the FTO/electrolyte decreased due to the compact TiO_2 blocking layer. Therefore, more electrons accumulated in the TiO_2 nanoparticle layer, thereby resulting in higher photovoltaic voltage concurrently. The decay-time constants were calculated to quantify the decay rate from equation [37]:

$$\tau = -\frac{k_B T}{e}\left(\frac{dV_{oc}}{dt}\right)^{-1}. \quad (1)$$

The decay-time constant of the blocking-layer (30 nm) coated sample is approximately one order of magnitude higher compared with bare sample at all the voltages, as shown in Fig. 4(b).

To examine the electrolyte reactions with FTO, cyclic voltammetry was performed in the same polysulfide electrolyte used in our QDSCs, as shown in Fig. 5. The TiO_2 blocking layer effectively suppresses oxidation/reduction reactions of the polysulfide electrolyte with the FTO. On the other hand, in the middle of the potential range, the capacitive current increases as the blocking layer becomes thicker, as clearly shown in the magnified inset of Fig. 5. The TiO_2 conduction-band position in the polysulfide electrolyte is estimated to be −0.83 V vs. NHE, based on measuring the acidity of the electrolyte (pH 12.1) with −0.12 V vs. NHE at pH 0

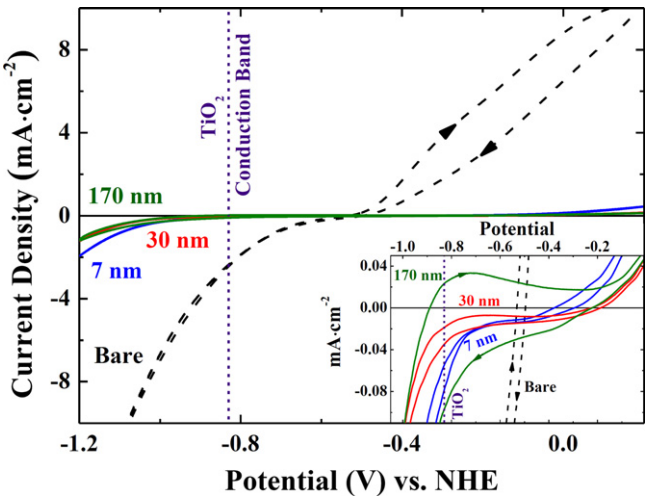

Fig. 5. Cyclic voltammetric curves of the bare and TiO_2 blocking-layer coated FTO electrode in the polysulfide electrolyte. The TiO_2 conduction-band position is illustrated as a short-dashed line.

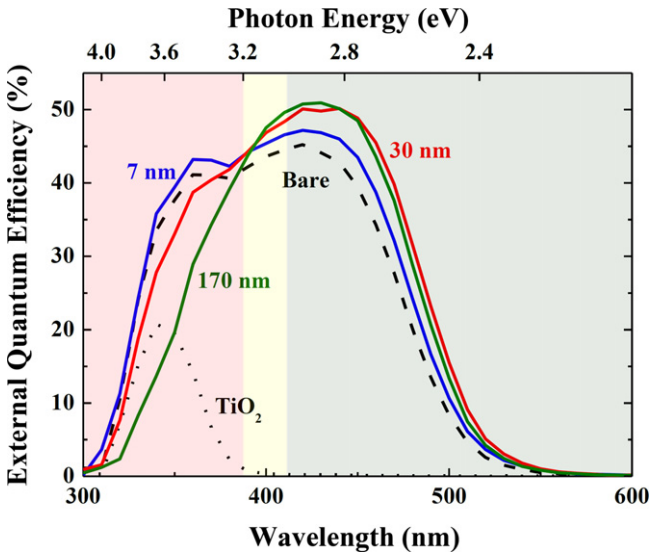

Fig. 6. Incident photon-to-current conversion efficiency (IPCE) spectra of QDSCs with various blocking-layer thicknesses. The IPCE of TiO_2 nanoparticles without CdS-sensitizer is shown as a dotted line.

for the conduction band of TiO_2 [38]. Therefore, we conclude that the capacitive current observed above −0.83 V is attributed to the filling of conduction-band states. Also, in the more positive potential region, capacitive current is still observed, due to a reversible filling of charge-trap states within the TiO_2 bandgap of the blocking layer [39,40]. These defects can act as recombination centers, which give rise to electron leakage by transferring photoexcited electrons from the TiO_2 blocking layer to the polysulfide electrolyte before reaching the FTO. In Fig. S2, the trap states are also observed in the absorption spectrum below the TiO_2-bandgap energy (3.2 eV), exhibiting an increased value with the thick blocking layer.

In order to characterize the light-harvesting effect of the blocking layer, we performed IPCE measurements, as shown in Fig. 6. Interestingly, asymmetric enhancement of IPCE is observed for the thick blocking-layer sample, which is not observed in the DSSCs. This is due to the absorption natures of the CdS semiconductor, and the trap-state absorption of the TiO_2 blocking layer. In the case of DSSCs, an IPCE below the ~390 nm region (left region) is mainly affected by the absorption from the bandgap of the TiO_2 nanoparticles [41] because the molar absorption coefficient of the dye ($\sim 10^4\ M^{-1}\ cm^{-1}$) is much lower than that of the TiO_2 [42]. In contrast, semiconductor quantum dots have much higher absorption coefficients of 10^5 to $10^6\ M^{-1}\ cm^{-1}$ [42] above the bandgap energy. Therefore, the values of the IPCE are represented by the summation of the CdS and TiO_2 responses in the UV region. As the TiO_2 blocking-layer thickness increases, more photons are absorbed by the TiO_2 layer. The TiO_2 nanoparticles without the CdS sensitizer in the polysulfide electrolyte, however, exhibit lower solar-cell performance in the UV region (over the TiO_2 bandgap or left region in Fig. 6). Furthermore, as the blocking layer becomes thicker, the slopes of the IPCE spectra become steeper below the bandgap energy (middle region) in Fig. 6. The reason for this is that the thicker blocking layer has much more trap states, which means that the absorption near the conduction band becomes intensified, as shown by the absorption spectra of Fig. S2. In the higher wavelength region (right region), symmetric enhancement of the IPCE is observed because the absorption through the TiO_2 blocking layer becomes insignificant.

Fig. 7 shows a schematic illustration for the effect of the blocking layer. The electron recombination from the FTO electrode to the polysulfide electrolyte is blocked by the addition of the compact TiO_2 blocking layer, thereby improving V_{oc}, I_{sc}, and the fill factor. Consequently, this phenomenon has a direct impact on the improved energy-conversion efficiency of the QDSCs.

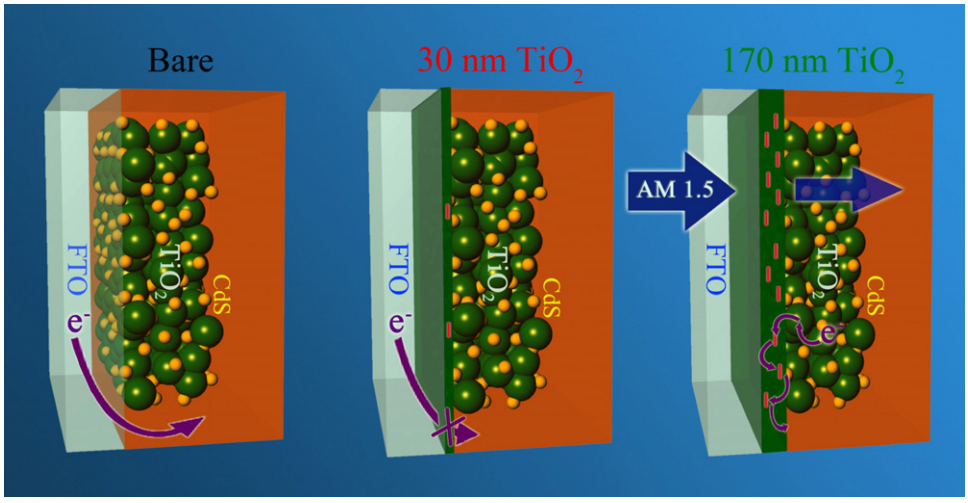

Fig. 7. Schematic figures of the TiO_2 blocking-layer effects on the performance of CdS-sensitized solar cells.

Nevertheless, when the blocking layer becomes too thick, the layer acts as trap sites for both recombination of the carrier and absorption of light. Therefore, the performance of the solar cell with the 170 nm blocking layer deteriorates.

4. Conclusions

The addition of blocking layer to QDSCs plays an important role in reducing the electron-carrier recombination at the FTO/electrolyte interface. The TiO_2 blocking-layer coated CdS-sensitized solar cell exhibits enhanced conversion efficiency compared with the bare cell by more than a factor of two. In contrast to DSSCs, asymmetric enhancement of the IPCE is also observed, due to the high extinction coefficients of the semiconductor quantum dots compared with that of dye molecules.

Acknowledgments

This research was supported by the National Research Foundation of Korea, through the World Class University (WCU, R31-2008-000-10075-0), and the Korean Government (MEST: NRF, 2010-0029065).

Appendix A. Supplementary data

Supplementary data associated with this article can be found, in the online version, at doi:10.1016/j.jpowsour.2011.08.052.

References

[1] B. O'Regan, M. Grätzel, Nature 353 (1991) 737–740.
[2] M.A. Green, K. Emery, Y. Hishikawa, W. Warta, Prog. Photovolt. Res. Appl. 19 (2011) 84–92.
[3] S. Ruhle, M. Shalom, A. Zaban, ChemPhysChem 11 (2010) 2290–2304.
[4] G. Hodes, J. Phys. Chem. C 112 (2008) 17778–17787.
[5] R.J. Ellingson, M.C. Beard, J.C. Johnson, P. Yu, O.I. Micic, A.J. Nozik, A. Shabaev, A.L. Efros, Nano Lett. 5 (2005) 865–871.
[6] D.-R. Jung, J. Kim, B. Park, Appl. Phys. Lett. 96 (2010) 211908.
[7] J.B. Sambur, T. Novet, B.A. Parkinson, Science 330 (2010) 63–66.
[8] Q. Zhang, X. Guo, X. Huang, S. Huang, D. Li, Y. Luo, Q. Shen, T. Toyoda, Q. Meng, Phys. Chem. Chem. Phys. 13 (2011) 4659–4667.
[9] I. Mora-Seró, S. Gimenez, F. Fabregat-Santiago, R. Gomez, Q. Shen, T. Toyoda, J. Bisquert, Acc. Chem. Res. 42 (2009) 1848–1857.
[10] I. Mora-Seró, J. Bisquert, J. Phys. Chem. Lett. 1 (2010) 3046–3052.
[11] S.M. Prokes, J.L. Gole, X.B. Chen, C. Burda, W.E. Carlos, Adv. Funct. Mater. 15 (2005) 161–167.
[12] E.C. Nelson, P.V. Braun, Science 318 (2007) 924–925.
[13] P. Ardalan, T.P. Brennan, H.-B.-R. Lee, J.R. Bakke, I.-K. Ding, M.D. McGehee, S.F. Bent, ACS Nano 5 (2011) 1495–1504.
[14] M. Shalom, S. Dor, S. Ruhle, L. Grinis, A. Zaban, J. Phys. Chem. C 113 (2009) 3895–3898.
[15] J.-Y. Hwang, S.-A. Lee, Y.H. Lee, S.-I. Seok, Appl. Mater. Interfaces 2 (2010) 1343–1348.
[16] Z. Liu, M. Miyauchi, Y. Uemura, Y. Cui, K. Hara, Z. Zhao, K. Sunahara, A. Furube, Appl. Phys. Lett. 96 (2010) 233107.
[17] S.M. Waita, B.O. Aduda, J.M. Mwabora, G.A. Niklasson, C.G. Granqvist, G. Boschloo, J. Electroanal. Chem. 637 (2009) 79–83.
[18] B. Yoo, K.-J. Kim, S.-Y. Bang, M.J. Ko, K. Kim, N.-G. Park, J. Electroanal. Chem. 638 (2010) 161–166.
[19] J. Xia, N. Masaki, K. Jiang, S. Yanagida, J. Phys. Chem. C 111 (2007) 8092–8097.
[20] N. Koide, A. Islam, Y. Chiba, L. Han, J. Photochem. Photobiol. A 182 (2006) 296–305.
[21] N. Fuke, L.B. Hoch, A.Y. Koposov, V.W. Manner, D.J. Werder, A. Fukui, N. Koide, H. Katayama, M. Sykora, ACS Nano 4 (2010) 6377–6386.
[22] Z. Yang, C.-Y. Chen, C.-W. Liu, H.-T. Chang, Chem. Commun. 46 (2010) 5485–5487.
[23] H. Lee, H.C. Leventis, S.-J. Moon, P. Chen, S. Ito, S.A. Haque, T. Torres, F. Nuesch, T. Geiger, S.M. Zakeeruddin, M. Grätzel, K. Nazeeruddin, Adv. Funct. Mater. 19 (2009) 1–8.
[24] Y.-L. Lee, C.-H. Chang, J. Power Sources 185 (2008) 584–588.
[25] Y. Zhao, X. Sheng, J. Zhai, L. Jiang, C. Yang, Z. Sun, Y. Li, D. Zhu, ChemPhysChem 8 (2007) 856–861.
[26] A. Hagfeldt, G. Boschloo, L. Sun, L. Kloo, H. Pettersson, Chem. Rev. 110 (2010) 6595–6663.
[27] H. Imahori, T. Umeyama, J. Phys. Chem. C 113 (2009) 9029–9039.
[28] J. Grandidier, D.M. Callahan, J.N. Munday, H.A. Atwater, Adv. Mater. 23 (2011) 1272–1276.
[29] P.J. Cameron, L.M. Peter, J. Phys. Chem. B 107 (2003) 14394–14400.
[30] C.-H. Lin, S. Chattopadhyay, C.-W. Hsu, M.-H. Wu, W.-C. Chen, C.-T. Wu, S.-C. Tseng, J.-S. Hwang, J.-H. Lee, C.-W. Chen, C.-H. Chen, L.-C. Chen, K.-H. Chen, Adv. Mater. 21 (2009) 759–763.
[31] V. González-Pedro, X. Xu, I. Mora-Seró, J. Bisquert, ACS Nano 4 (2010) 5783–5790.
[32] Y. Park, B. Lee, C. Kim, J. Kim, S. Nam, Y. Oh, B. Park, J. Phys. Chem. C 114 (2010) 3688–3692.
[33] J. Cho, Y.-W. Kim, B. Kim, J.-G. Lee, B. Park, Angew. Chem. Int. Ed. 42 (2003) 1618–1621.
[34] F. Fabregat-Santiago, J. Bisquert, E. Palomares, L. Otero, D. Kuang, S.M. Zakeeruddin, M. Grätzel, J. Phys. Chem. C 111 (2007) 6550–6560.
[35] F. Fabregat-Santiago, J. Bisquert, G. Garcia-Belmonte, G. Boschloob, A. Hagfeldt, Sol. Energy Mater. Sol. Cells 87 (2005) 117–131.
[36] R. Kern, R. Sastrawan, J. Ferber, R. Stangl, J. Luther, Electrochim. Acta 47 (2002) 4213–4225.
[37] A. Zaban, M. Greenshtein, J. Bisquert, ChemPhysChem 4 (2003) 859–864.
[38] D. Duonghong, J. Ramsden, M. Grätzel, J. Am. Chem. Soc. 104 (1982) 2977–2985.
[39] Z. Zhang, S.M. Zakeeruddin, B. O'Regan, R. Humphry-Baker, M. Grätzel, J. Phys. Chem. B 109 (2005) 21818–21824.
[40] T. Berger, T. Lana-Villarreal, D. Monllor-Satoca, R. Gómez, J. Phys. Chem. C 111 (2007) 9936–9942.
[41] M. Grätzel, J. Photochem. Photobiol. C 4 (2003) 145–153.
[42] T. Miyasaka, J. Phys. Chem. Lett. 2 (2011) 262–269.